The Reconstruction of The Effective Attenuation Coefficient Using Optoacoustic Simulations

Submitted by:

Liad Ben Shachar

Contents

Abstract

In this paper, we tried to use optoacoustics to reconstruct a tissue's effective attenuation coefficient. We used the ValoMC software for Monte Carlo photon transport simulation, and the K-Wave package for a forward and backward simulation of optoacoustics. Using these, we created different scenarios, and tried to reconstruct for each, the coefficient. The method of reconstruction we used was quite simplistic and took advantage of many approximations.

Our findings demonstrate that the reconstruction is quite robust to variance in the medium, and even to distinct and different regions. However, when tackled with the realistic scenario of successive layers, and regions which are near the surface, the simplistic reconstruction fails, as do the approximations. We conclude that for most realistic scenarios, a better approximation and a more complicated reconstruction method are needed.

1 Introduction

Biological tissues, like many other mediums, scatter and absorb light. Different tissues absorb and scatter light differently. Furthermore, these properties are dependent on the light's wavelength. In the field of medical imaging it can be very useful to know the values of these properties. For example, tumors usually have different properties than the surrounding tissue [1].

One difficulty of assessing these properties is that they cannot be measured directly. Fortunately, the absorption and scattering coefficient, μ_a and μ_s respectively, can be extracted using a combination of other measurable properties. One such property is the effective attenuation coefficient μ_{eff}.

In addition to its use in obtaining μ_a and μ_s, it is valuable to know how the light decays in a tissue as a function of wavelength.

1.1 The Radiative Transfer Equation

The equation that governs light propagation in scattering and absorbing mediums is the **Radiative Transfer Equation** (RTE). The full equation is

$$\frac{1}{c}\frac{d}{dt}I\left(r,t,\hat{s}\right)+\frac{d}{d\hat{s}}I\left(r,t,\hat{s}\right)+\mu_t(r)I\left(r,t,\hat{s}\right)-\mu_s(r)\int\limits_{4\pi}I\left(r,t,\hat{s'}\right)p\left(\hat{s'},\hat{s}\right)d\Omega'=\epsilon\left(r,t,\hat{s}\right)$$

Where $I(r,\hat{s})$ is the radiance in location r and direction $\hat{s}$, c the speed of light, $\mu_t(r)$ is the attenuation coefficient:

$$\mu_t(r)=\mu_a(r)+(1-g)\cdot\mu_s(r)$$

where g is the anisotropic factor, and μ_a and μ_s as defined before. $p(\hat{s'},\hat{s})$ is the phase function which tells the probability of scattering from $\hat{s'}$ to $\hat{s}$, and $\epsilon(r,\hat{s})$ is a possible input radiance.

1.1.1 The Diffusion Approximation

We will skip the development of the diffusion approximation. Further development can be seen in [8]. The Green function of the diffusion approximation in DC is:

$$G = \frac{e^{\mu_{eff}|r-r'|}}{4\pi\left|r-r'\right|}$$

Where:

$$\mu_{eff} = \sqrt{3 \cdot (\mu_a + (1-g)\cdot\mu_s)}$$

For an infinite half space, with a point source at $x = 0$, where x is the depth axis, we will get the following Green function:

$$G(x,\rho) = \frac{1}{4\pi D}\left(\frac{e^{-\mu_{eff}\sqrt{(x-l)^2+\rho^2}}}{\sqrt{(x-l)^2+\rho^2}} - \frac{e^{-\mu_{eff}\sqrt{(x+l+2D)^2+\rho^2}}}{\sqrt{(x+l+2D)^2+\rho^2}}\right)$$

Where D is the diffusion coefficient, and l is the the typical diffusion length, as in how deep does the light penetrates before the diffusion approximation is applicable. Their values are:

$$l = \frac{1}{\mu_a + (1-g)\cdot\mu_s} \quad , \quad D = \frac{1}{3 * (\mu_a + (1-g)\cdot\mu_s)}$$

1.2 1D approximation

In order to simplify this equation, we try to illuminate the medium with a wide illumination. Thus:

$$S_0 = \begin{cases} \delta(x) & \rho < R \\ 0 & else \end{cases}$$

Therefore, the solution would be:

$$U(r) = \int_0^R \int_0^\pi G(x,\rho)\,\rho d\rho d\theta$$

For a larger discussion about a finite light source, and the needed radius for the approximation, see Appendix. For now we will take $R \to \infty$.

$$U(r) = \int_0^R \int_0^\pi \frac{1}{4\pi D}\left(\frac{e^{-\mu_{eff}\sqrt{(x-l)^2+\rho^2}}}{\sqrt{(x-l)^2+\rho^2}} - \frac{e^{-\mu_{eff}\sqrt{(x+l+2D)^2+\rho^2}}}{\sqrt{(x+l+2D)^2+\rho^2}}\right)\rho d\rho d\theta \tag{1}$$

$$U(r) = -\frac{1}{2D\mu_{eff}}\left(e^{-\mu_{eff}\sqrt{(x-l)^2+\rho^2}} - e^{-\mu_{eff}\sqrt{(x+l+2D)^2+\rho^2}}\right)\Bigg|_0^\infty \tag{2}$$

$$U(r) = \frac{1}{2D\mu_{eff}}\left(e^{-\mu_{eff}|x-l|} - e^{-\mu_{eff}|x+l+2D|}\right) \tag{3}$$

Assuming that $x > l > 0 > -l - 2D$ this can be written as:

$$U(r) = \frac{1}{2D\mu_{eff}} \left(e^{-\mu_{eff}(x-l)} - e^{-\mu_{eff}(x+l+2D)} \right) \tag{4}$$

$$U(r) = \frac{1}{2D\mu_{eff}} e^{-\mu_{eff}x} \left(e^{\mu_{eff}l} - e^{-\mu_{eff}(l+2D)} \right) \tag{5}$$

This is an exponent! Therefore, if we use a wide enough light source, and we examine the depth where $x > l$ we should find that the fluence behave likes an exponent with regards to x, where the coefficient is μ_{eff}. Notice that even though now the problem is practically 1D, the μ_{eff} doesn't change.

Therefore, if we could somehow obtain the light profile in a medium, it should theoretically be possible to find the effective attenuation. One possible way to do this is with Optoacoustics.

1.3 Optoacoustic Reconstruction

The **Optoacoustic Effect** or **Photoacoustic Effect** refers to the effect of generating sound wave using light. The basic explanation is that absorbed light causes a medium to heat and expand, generating pressure waves. The solution for absorbed energy of the form $H(r,t) = H(r) \cdot \delta(t)$ is

$$p(r, t = 0) = \Gamma H(r)$$

Where $p(r,t)$ is the pressure, Γ is the grüneisen coefficient and H is the absorbed energy by the medium. Therefore, if we record the acoustic wave coming from a medium after illumination, we might be able to reconstruct the absorbed energy. One method of reconstruction is the **Frequency-Domain solution**. In short, using the sensors on a line in the y axis (in the case of the 2D problem) we obtain $p(y,t)$. Applying a Fourier transform we get $P(k_y, \omega)$, Then, we can transform to $P(k_x, k_y)$ using the known dispersion relation $\omega = v\sqrt{k_x^2 + k_y^2}$. Applying the inverse Fourier transform we will get $p(x,y)$. Some details have been glossed over, such as why would this $p(x,y) = p(x,y,t = 0)$. A full discussion of the algorithm can be seen in [3]. Dividing $p(x,y,t=0)$ by Γ we will obtain $H(r)$. This is the *light absorption map*. It is not the same as the light profile, but if we assume that μ_a is constant in the medium, it means that it is proportional to the light profile. Thus, they will have the same effective attenuation factor. we will only work with the light absorption map.

The Limited View Problem: The limited view problem is a common problem in optoacoustic tomography. The fact that we usually cannot enclose a tissue with sensors, causes some spacial frequencies not to be detected.

1.4 Monte Carlo Method

One method of simulating light propagation in a medium is the **Monte Carlo Method**. In this method, photon packets are simulated to be passing through the medium. The probabilities of absorbing a packet or scattering it in a certain direction are based on the local parameters. In this manner we get the full trajectory of a photon packet. Averaging

over all photon packet trajectories, we will get a very good approximation for the solution to the RTE. The more packets, the more it converges to the actual solutions. For a full explanation of the Monte Carlo method for photon transport, see [7].

Notice, that while we use the **Diffusion Approximation** for analytical expressions, we will actually use Monte Carlo simulations, as they are more precise. This means that our analytical expressions will not work in areas where the depth is less than the diffusion length l.

2 Method

The following section details our experiment's parameters and methods. We performed the simulations on a 2D grid, for ease of computation. The code was written in Matlab and is available at our git repository: `https://github.com/liad95/absorbtion-coef`

2.1 Monte Carlo Light Propagation

In order to generate a light absorption map, we used the *Monte Carlo* method for photon transport. Specifically, we used the ValoMC software to simulate the photon transport in our slab [**ValoMC**]. In order to perform the simulation, ValoMC must have the medium properties, namely the absorption coefficient map, the scattering coefficient map and the refractive index map. Therefore, after defining these, and the light sources, we could run the simulation.

2.2 K-Wave Forward and Backward

After acquiring the light absorption map from the ValoMC simulation, a simple multiplication with the grüneisen coefficient granted us the initial pressure map. We then used the K-Wave toolbox in order to solve the **forward and backward problems** [2].

The **forward problem** is, given the initial pressure and and the speed of sound in the medium, how would the acoustic wave propagate through the system? Using K-Wave, we also defined locations of acoustic sensors, which recorded the pressure at those locations as a function of time.

The **backward problem** is, given the sensors' locations and recordings and the speed of sound in the medium, what is the initial pressure? This is also called the **tomographic problem**. In order to solve this, the K-Wave package implements the frequency-domain solution which was previously introduced.

Dividing the reconstructed initial pressure by the grüneisen coefficient we acquired the light absorption map.

2.3 Reconstruction Method

Once we have an absorption map, either from the K-Wave package using the grüneisen coefficient, or from the ValoMC simulation, we can perform a simple regression in order to reconstruct the μ_{eff}.

As we have discussed, with the use of several approximation, we can assume that the light decays exponentially. We constructed our scenarios such that these approximations would hold. Thus, we performed a linear regression on $\log H$, taking the slope parameter to be the reconstructed decay coefficient μ_{eff}. Specifically, we perform regression on the section of the absorption map which "behaves" the most exponential. Currently, we find these area by sight. Further development is needed to find them automatically.

In addition, we performed the regression both on the center line of the simulation, and on a cylinder ,(square in 2D) with radius r from the center line. This produced 2 separate results.

Notice: Only reconstruction using the K-Wave results is realistic. Reconstructions from the ValoMC results were only done for verification and debugging.

3 Configuration

Going into the details about the specific experiments and simulations, we will first discuss the specifics about the setup:

3.1 ValoMC Setup

For the ValoMC medium we defined a 2D matrix of $201X101$ elements, with $dx = 0.05[mm]$, $dy = 0.5[mm]$. Overall the slab is of size $10X50[mm^2]$. The base absorption and scattering coefficient are $\mu_{\text{a}} = 0.01[mm^{-1}]$, $\mu_{\text{s}} = 10[mm^{-1}]$, with anisotropy factor $g = 0.9$ and grüneisen coefficient of 0.5. The illumination is a direct light source, with a diameter of $49[mm]$. The photon count was either set to 10^9 or 10^8. Will be specified in each experiment. 10^8 is more than enough photon packets, but we have unfortunately learned this quite late in the process.

3.1.1 Light Source Diameter

The larger the diameter, the better the 1D approximation is. A full discussion about minimizing error as a function of the diameter can be seen in the appendix. We tested the effect of the light source size, on the reconstruction from ValoMC simulation (we didn't want the properties of the acoustic sensors to interfere with the analysis). As discussed, we performed 2 linear regressions. One for the center line only, and another for the cylinder with radius $r = 3[mm]$ around the center line. Figure 1 shows a comparison of the ratio between each of these values and the theoretical value as a function of the diameter of the light source, in dB. As in

$$y = 20 \cdot \log_{10}\left(\frac{\mu_{eff,regression}}{mu_{eff,theoretical}}\right)$$

The figure also displays the normalized value we expect to find by using a regression with a finite illumination. As we showed in the appendix, the expression for the derivative of the illumination is:

$$= \mu_{eff}\left[-1 + \frac{\left(e^{-\mu_{eff}\sqrt{(x-l)^2+R^2}}\right)}{1 - e^{-\mu_{eff}\sqrt{(x-l)^2+R^2}}}\left(\frac{x-l}{\sqrt{(x-l)^2+R^2}} - 1\right)\right]$$

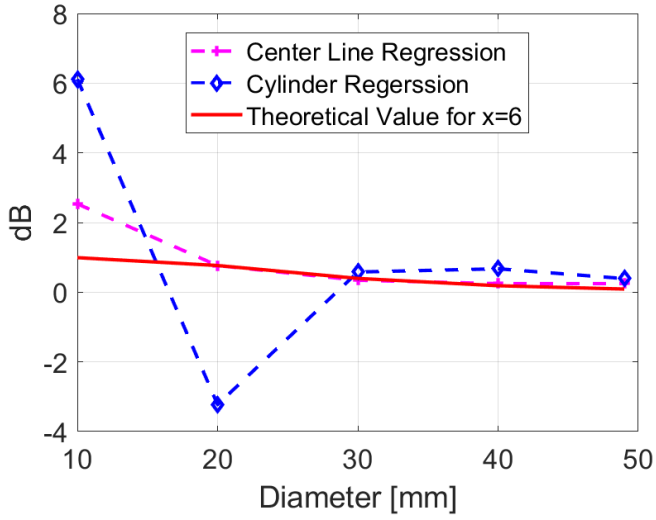

Figure 1: Ratio of reconstructed and theoretical μ_{eff} vs the radius of the light source, for different reconstruction methods. Also displays the theoretical value of this ratio

In the normalized dB graph this will be:

$$20 \cdot \log_{10}\left(\left|-1+\frac{\left(e^{-\mu_{eff}\sqrt{(x-l)^2+R^2}}\right)}{1-e^{-\mu_{eff}\sqrt{(x-l)^2+R^2}}}\left(\frac{x-l}{\sqrt{(x-l)^2+R^2}}-1\right)\right|\right)$$

We chose $x = 6[mm]$ as it is the middle of the regression. We can see that it matches the value we reconstructed quite well, except for smaller diameters. This could be because when the diameter is not large in comparison to x the derivative itself is not quite constant, and taking one point on it is not a good approximation to a fit result. We can see that we get a good approximation for $D \geq 30[mm]$. The light source for the following experiment is a direct light source with a diameter of $49[mm]$.

3.2 K-Wave Setup

We set up a line of 5 sensors arranged in the middle of the y axis. The distances are the same as the ValoMC pixels, meaning $dy = 0.5[mm]$. The speed of sound in the medium was set to $1500[m/s]$ and its density to $1000[kg/m^3]$. The perfectly matched layer (PML) was set to be outside the bounds of the simulation.

3.2.1 Aperture Size

You will notice that the sensor aperture is quite small compared to the slab size. We did try working with a larger aperture, but it did not yield good results. These results can be seen in Figure 2. The x axis here is the number of tightly packed sensors (as in dy of sensors is the same as the dy of the ValoMc and K-Wave grid). The smaller one performed better, we assume because of the limited view problem. As we shrunk the aperture, less information would came from the periphery of the slab, where the illumination was not ideally uniform. Thus, choosing the sensor grid size to be 5 pixels, the K-Wave reconstruction would reconstruct it completely uniform in the y axis (as seen in 9 for example).

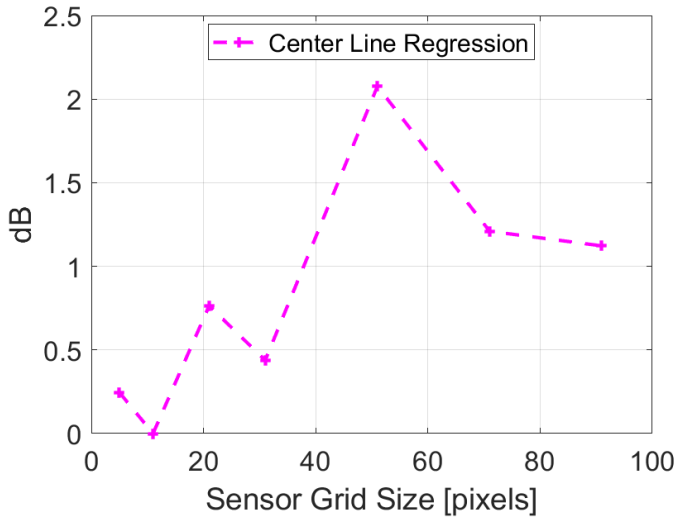

Figure 2: Ratio of reconstructed and theoretical μ_{eff} vs the sensor grid size in pixels, for the Center Line reconstruction methods.

4 Experiments

Using these setups, or similar setups (differences will be mentioned), we ran several experiments:

4.1 Gaussian Variation

In order to better simulate actual tissue materials, when defining the scattering and absorption matrices for the ValoMC simulation, we introduced a variance in the values like so:

$$\text{Absorpbtion Matrix} = \mu_a + \mu_a \sigma N$$

$$\text{Scattering Matrix} = \mu_s + \mu_s \sigma N$$

Where N is a sampling from a normal distribution. When elements of the either matrix turned out negative we set the element to 0. We analyzed the quality of the reconstruction as a function of σ.

4.2 Correlated Variation

In this experiment we applied a Gaussian filter to the sampled normal distribution. We did this, to better simulate realistic variation, which we would assume to have some spacial correlation. Specifically:

$$\text{Absorpbtion Matrix} = \mu_a + \mu_a \sigma \cdot \text{Filter}(N)$$

$$\text{Scattering Matrix} = \mu_s + \mu_s \sigma \cdot \text{Filter}(N)$$

Where the Gaussian filter is defined with filter size of 10, and a sigma of 2. An example image of Filter(N) can be seen in figure 3.

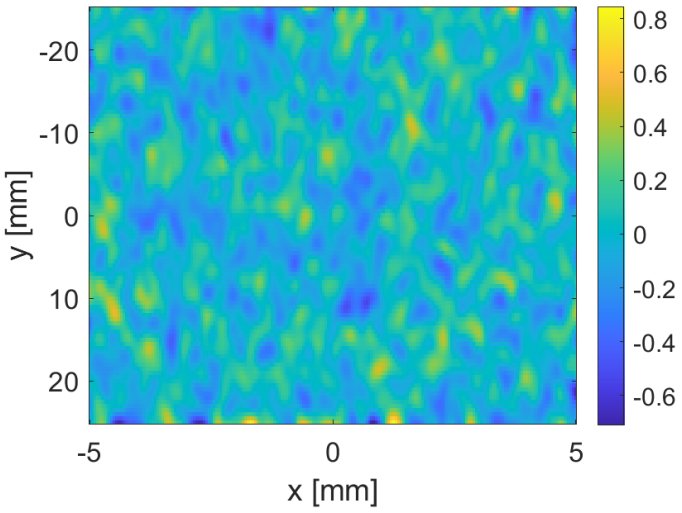

Figure 3: An example of Filter(N)

4.3 Ellipses

The Variation experiments tests the robustness of the reconstruction to small variations due to inherent lack of perfection in physical mediums. We also wanted to find the robustness to large amounts of in-homogeneity in the tissue. Therefore, we enclosed a separate elliptical medium inside the slab, in different locations, and with different absorption coefficient:

$$\text{Absorpbtion Matrix} = \mu_a + \mu_a * \sigma * N + q * \mu_a * \text{createEllipse}()$$

Where createEllipse() is a function that returns an ellipse, and q is a multiplier that we varied in order to exaggerate the absorption of the ellipse .The scattering map was left unchanged. We constructed 4 different Ellipse tests, where in each one the ellipse is located and oriented differently. For ease we defined: test A, test B ,test C, test D. In figure 4 we can see each ellipse's location and orientation. Later, we analyzed the quality of the reconstruction as a function of q and the locations of the ellipse.

4.4 2 Layers

Up until now we analyzed the scenario of a single layer, with quite a large thickness. However, tissues do not naturally exist like so. The dermis is usually a few millimeter thick, and the epidermis is less than a millimeter thick [5]. Even if we are discussing subcutaneous fat, which could reach a thickness of several centimeter [6] , it would be covered in other skin layers. Therefore, we tested 2 cases of a 2 layer medium. In the first case, the illuminated layer is thin ($3[mm]$) and the regression is performed on the second thicker layer. In the second case, the first layer is thicker and the regression is performed on it. In both cases the overall dimension are the same as for the single layer problem, as in overall thickness being $10[mm]$.

We kept the first layer's absorption coefficient constant, and varied the second layer's absorption coefficient. In Figure 5 we can see the setup of both experiments.

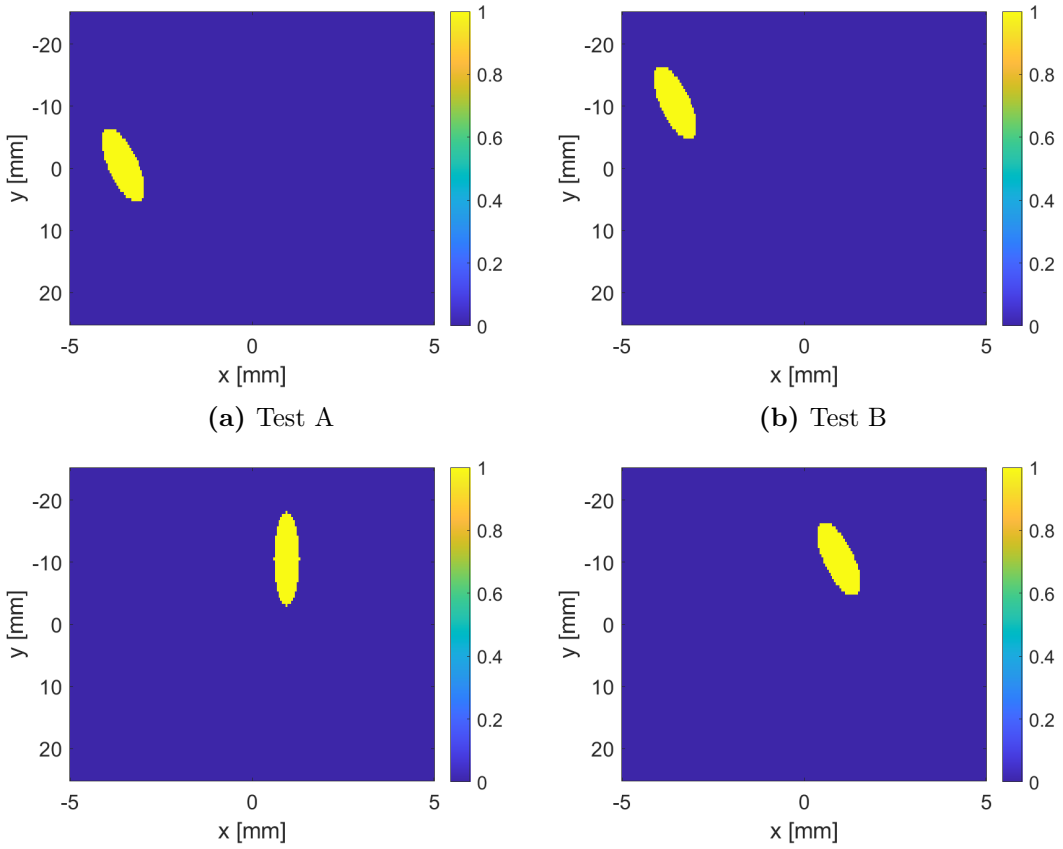

(a) Test A **(b)** Test B

(c) Test C **(d)** Test D

Figure 4: The Ellipse's location and orientation for tests A-D

Notice: In the *Close* experiment we reconstruct the μ_{eff} of the farther layer, and in the *Far* experiment we reconstruct the μ_{eff} of the closer layer. The names indicate how close the boundary is.

5 Results

5.1 Gaussian Variation

Before going into all of the experiments' results, let us examine a simple example.

5.1.1 example: $\sigma = 0$

In this section we will display our methodology. We ran the simulations on a completely homogeneous medium, and reconstructed μ_{eff}. The results from the ValoMC simulation can be seen in figure 6. From the absorption image **(a)** we can infer the radius of the light source. From the image of center line absorption plot **(b)** we can see at which depths the light behaves exponentially. This can be easily seen by the *log* plot. From this information, we decided the cutoff points of the regression, as seen in the green regression area. After performing the regression, and finding the fit plots, we compared them in the regression area **(c)**.

After simulating the energy absorption map, we multiplied it by the grüneisen coefficient

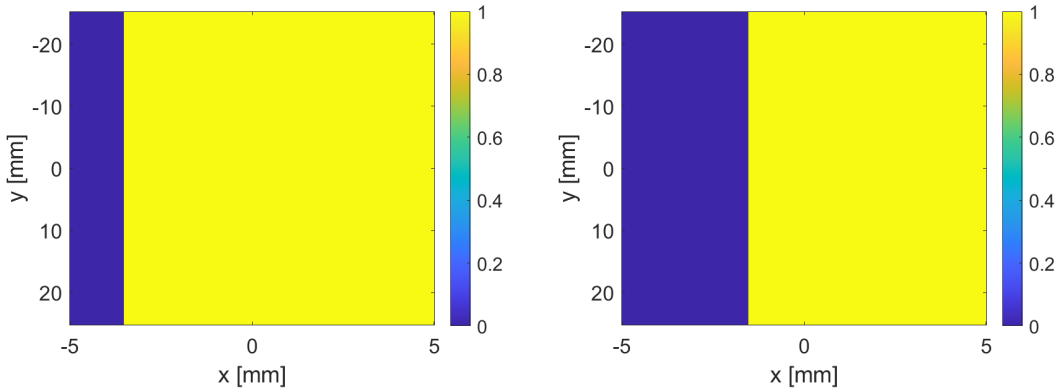

(a) Close Setup **(b)** Far Setup

Figure 5: The configurations of the 2 Layer experiments

to get the initial pressure. Then, after defining the acoustic sensor, and medium properties as mentioned in the previous section, we passed this to the K-Wave for simulation and then reconstruction (forward and backward). Dividing the reconstructed initial pressure by the grüneisen coefficient, we obtained the reconstruction of the absorbed energy. Then we applied the regression again. The results can be seen in figure 7. The graphs are of the same nature. One interesting detail, is that there is a smearing in the y axis, which means that now we cannot tell the radius of the light source.

Finally, we compared the reconstructed μ_{eff} from both the ValoMC simulation and the K-Wave reconstruction to the ground truth value. We also compared between the 2 regression methods. The comparison can be seen in table 1.

	Reconstruced μ_{eff}	Relative Error
ValoMC - Center	0.176	0.01
ValoMC - Cylinder	0.176	0.01
K-Wave - Center	0.177	0.01
K-Wave - Cylinder	0.176	0.01

Table 1: Ground Truth μ_{eff} Vs Reconstructed μ_{eff} comparison

In the following sections we will not display all of these graphs, unless they are of interest. The complete set of graphs and results can be found in the project's GitHub page, in the Analysis Results Folder.

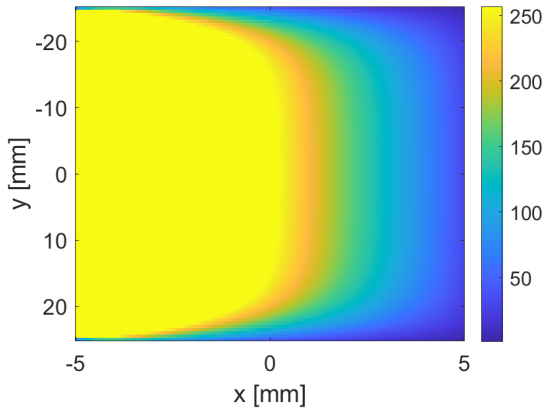

(a) ValoMC Absorption Map

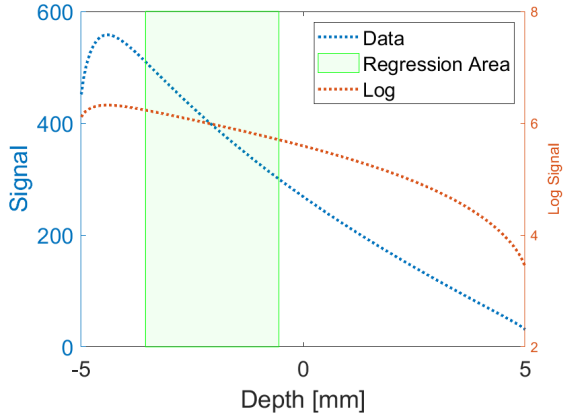

(b) ValoMC Center Line Absorption Plot

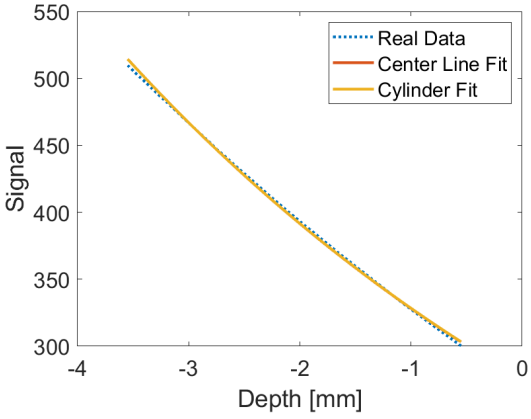

(c) Fit Comparisons in the Regression Area

Figure 6: Simulation and regression results for the homogeneous ValoMC simulation. **(a)** Absorption map of the slab. **(b)** The Absorption at the center line of the slab, and its *log*. The green patch denotes the region where we performed the regression. **(c)** Comparison of the simulated absorption with the fitted lines in the regression region.

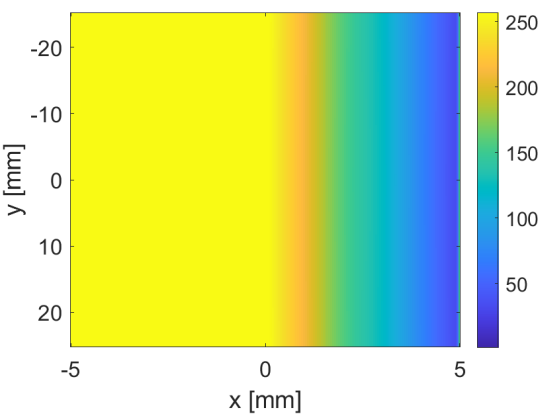

(a) K-Wave Absorption Map

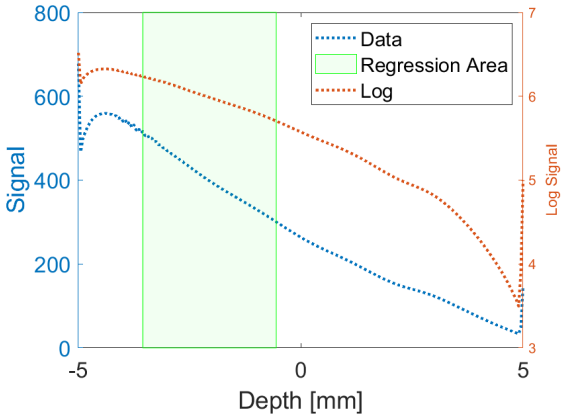

(b) K-Wave Center Line Absorption Plot

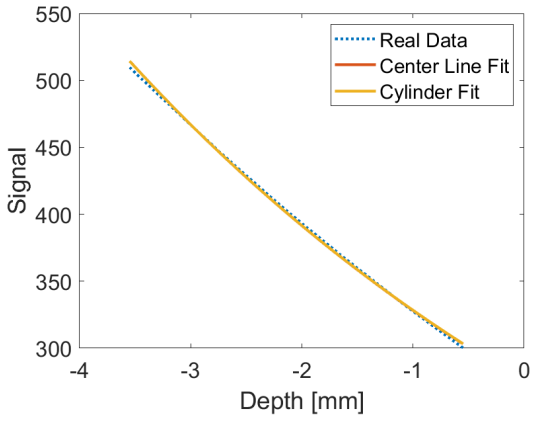

(c) Fit Comparisons in the Regression Area

Figure 7: Simulation and regression results for the homogeneous K-Wave simulation. **(a)** Absorption map of the slab. **(b)** The Absorption at the center line of the slab, and its *log*. The green patch denotes the region where we performed the regression. **(c)** Comparison of the simulated absorption with the fitted lines in the regression region.

5.1.2 Further Variations

After executing this baseline test, we set out to run the 2D Gaussian variation experiment as discussed above. In figure 8 we can see the absorption maps resulting from the ValoMC simulation for the different σ's. The circle source and the variation in absorption coefficient are all apparent from the images. However, after passing the simulation output through the forward and backward algorithms of the K-Wave we can see in figure 9 that the smearing effect in the y axis evens out the variance, at least in the y direction.

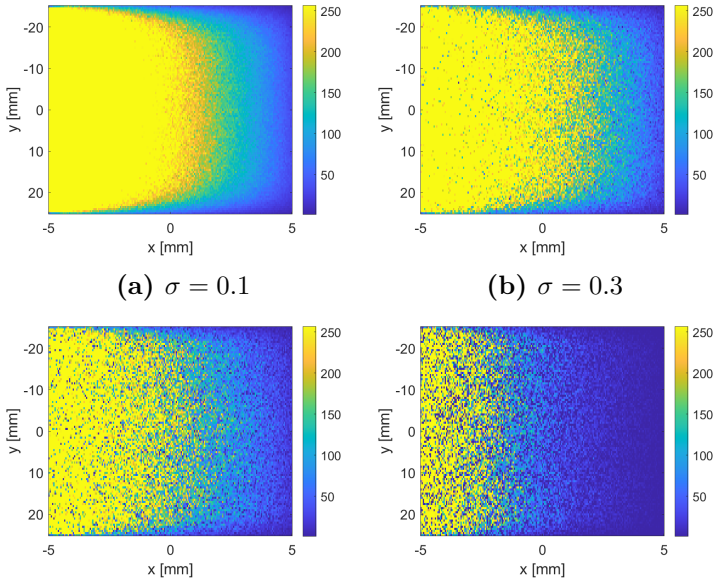

(a) $\sigma = 0.1$ **(b)** $\sigma = 0.3$

(c) $\sigma = 0.5$ **(d)** $\sigma = 1$

Figure 8: ValoMC absorption maps for the different variances σ defined

A comparison of the reconstructed μ_{eff} and the theoretical one can be seen in figure 10 for both regressions. We can see that for values of $\sigma \leq 0.3$ we get quite a small error (relative error less than 0.07).

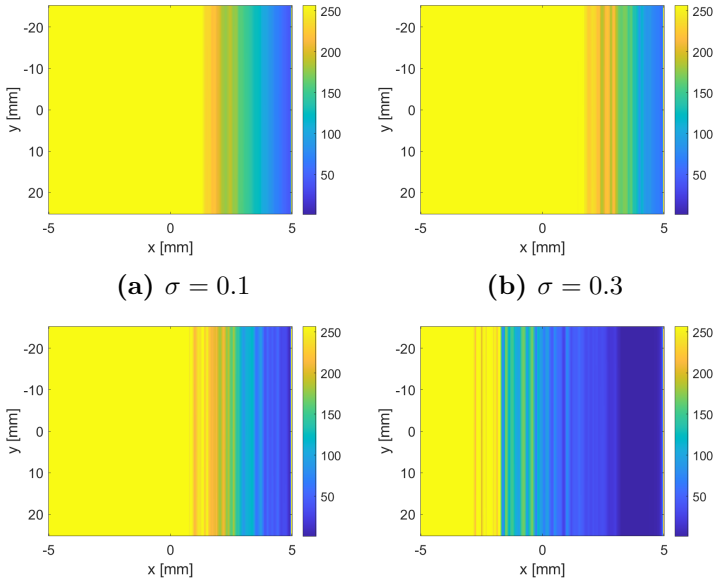

(a) $\sigma = 0.1$ **(b)** $\sigma = 0.3$

(c) $\sigma = 0.5$ **(d)** $\sigma = 1$

Figure 9: K-Wave absorption maps for the different variances σ defined

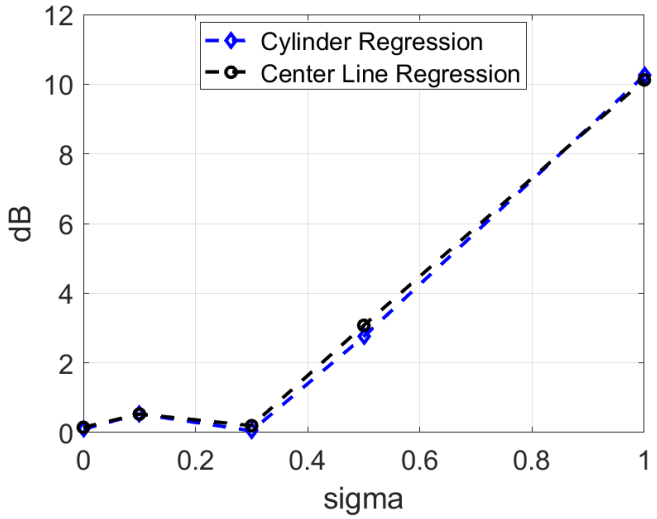

Figure 10: Ratio of reconstructed and theoretical μ_{eff} Vs the sigma of the Gaussian variation, for different reconstruction methods.

5.2 Correlated Gaussian Variation

In a very similar manner, we executed the Correlated Gaussian Variation experiment. A comparison of the reconstructed μ_{eff} and the theoretical one can be seen in figure 11. We see again that up to and including $\sigma = 0.3$ we get quite a decent Reconstruction (less than $1dB$).

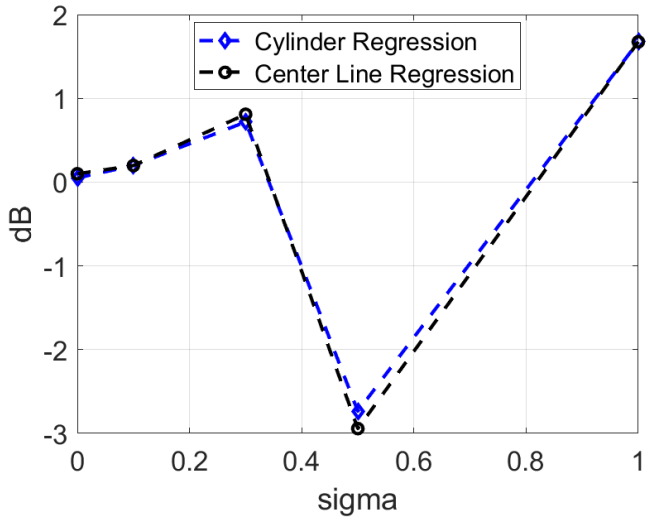

Figure 11: Ratio of reconstructed and theoretical μ_{eff} Vs the sigma of the correlated Gaussian variation, for different reconstruction methods

Furthermore, it is consistent across all tests that the Center Line and Cylinder regression produce the same result. Therefore, we will only display the Center result, for ease of reading. Again, the full results can be found in the GitHub page.

5.3 Ellipses

The previous results showed that we can deal with variations in the medium up to a certain degree. The ellipse tests examined a different scenario of a distinct different medium contained inside the medium of interest. We ran the 4 ellipse tests, A through D, and compared the reconstructed μ_{eff} for each test as a function of q, the ellipse relative absorption. The results can be seen in Figure 12.

We see from the figure that the regression somewhat works for tests B-D (up to $1dB$), however, the results for test A are significantly worse. This is probably because in test A the ellipse is directly in the middle of the illumination and it is very close to the light source. We will see a similar effect in our next experiment. It should be mentioned that increasing the radius of the regression cylinder did not yield better results.

5.3.1 2 Layers

For both 2 layer experiment, we obtained the ratio between the found and theoretical μ_{eff} as a function of the second layer's absorption coefficient $\mu_{a,2}$. The regression was always performed on the thicker layer, and compared to the thicker layer's theoretical effective attenuation coefficient $\mu_{eff,theo,thick}$. The comparison for both experiments can be seen in Figure 13.

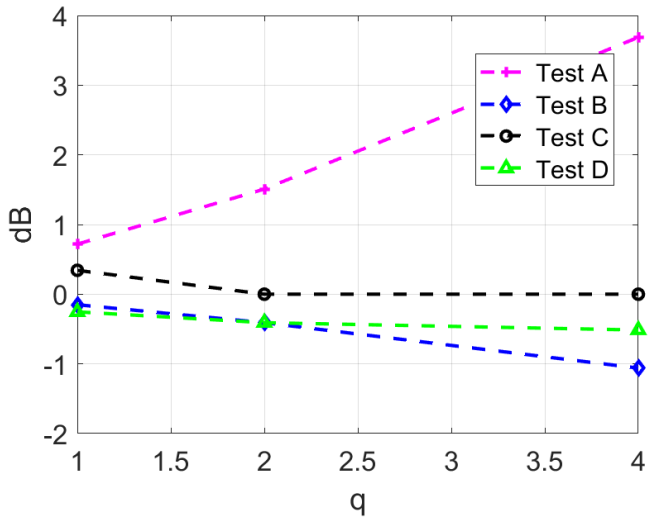

Figure 12: Ratio of reconstructed and theoretical μ_{eff} Vs the ellipse multiplier q, for the different ellipse tests

We can see that the reconstruction in *2nd Layer Far* is much better than the reconstruction in *2nd Layer Close*, but still not as good as the results for the previous experiments.

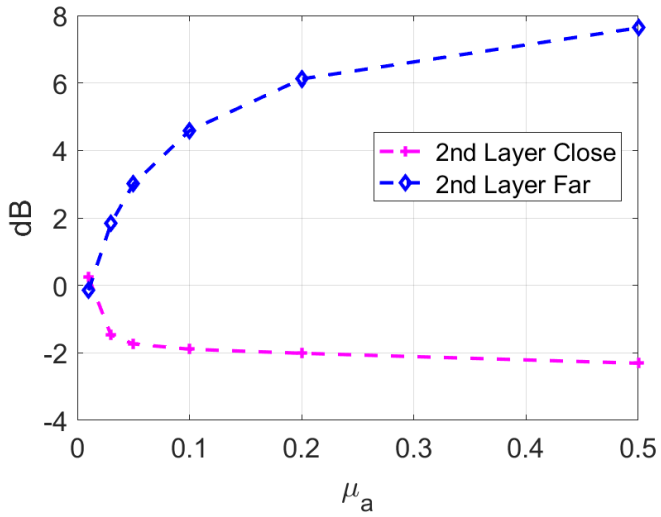

Figure 13: Ratio of reconstructed and theoretical μ_{eff} Vs the absorption coefficient μ_a of the second layer, for the 2 scenarios. For *2nd Layer Close* we find the μ_{eff} of the 2nd layer, and compare it to the 2nd layer's theoretical μ_{eff}. For *2nd Layer Far* we find the μ_{eff} of the 1st layer, and compare it to the 1st layer's theoretical μ_{eff}.

6 Discussion and Further Work

We have seen many results, let us try summarize and explain.

First of all, we can see that a decently small variation in the medium does not effect the overall results of the reconstructed effective attenuation factor. Even larger regions of variation, seen in the correlated variation experiment, did not ruin the Reconstruction for sufficiently low variation levels (up to $\sigma = 0.3$). Second of all, we can see that larger and more prominent regions did not interfere with the reconstruction, as seen in the ellipse tests B-D, and the *2nd Layer Far* to degree. However, ellipse test A, and the *2nd Layer Close* test resulted in the worse reconstructions we had. The mutual property between these 2 tests where how close the interference was to the front of the slab, and how close the interference was to the center of illumination. The fact that the interfering medium was near the front of the slab, could break our approximation, where we assume that the light profile is a single exponent. The second layer (either a full layer, or the ellipse) would cause other boundary conditions to arise, which could shift our simple solution to a more complicated one.

6.1 Limited View

The limited view effect has popped its head several times along the way. We can see its effect in the smoothing of the variance in the y direction in the K-Wave reconstruction images for the variance experiments. We can also see its effect in the fact that the Cylinder regression is almost identical to the Center Line regression, even if we enlarge the radius we are looking at, as mentioned in the results for the ellipse test A. The limited view effectively duplicated the center line across the slab, so no difference would be gain by looking at a larger portion of the slab. This is not a problem when the variance is low, or when the disturbance is far. It could even "wipe out" the effects of disturbances outside the field of view (close to the front of the slab and to the side). Unfortunately it

causes problems in the case where the disturbance is in the field of view and close to the front, such as in ellipse test A.

6.2 Further Work

It is pretty obvious that a better approximation is needed. A full diffusion solution to a multi-layered medium is needed in order to find the function to fit. The diffusion approximation should still hold in depths larger than the typical diffusion length, regardless of how close we are to a boundary, as once we pass this depth, the light should be completely diffusive/isotropic. A possible avenue for a better yet still simple solution could be based on work done by G.Domański Et al [4]. At the end of that article they also conclude that a better approximation is needed, however they used Diffuse Optics in order to reconstruct the value, and not Optoacoustics, which gives us a full image of the absorption. It should be noted that according to [8] (page R56) if the medium consists of several piecewise continuous regions the boundary conditions cannot be met exactly.

It could also be interesting to see if by moving the apparatus around (light source + sensors) and averaging the reconstructed effective attenuation coefficient we could get cancel effect of small disturbances such as ellipse test A. This would be analogous to moving the ellipse around in the medium, and averaging the resulting reconstructed coefficient. Another possible direction would be to have a very large aperture in order to better reconstruct the absorption map. Thus, we could perform the regression only on the section without the ellipse, and get a better result. Both of these methods would likely require a larger surface area. We might be able to make the light source smaller, in order to mitigate some of this, according to Figure 1 in the appendix.

7 Conclusions

We tackled the problem of obtaining the effective attenuation coefficient with optoacoustic imaging. In order to simplify our problem we used several approximations: the diffusion approximation, uniform lighting (1D) and that the diffusion solution is a single exponent. By analyzing the effect of the illumination radius, and by testing various radii and various sensor sizes, we chose our simulation parameters. With these approximations and simulation parameters, we managed to reconstruct the coefficient in some simulated scenarios.

In cases with moderate variation in the medium, and in cases where distinctly different regions where not close to the illumination center, the reconstruction worked well. However, in cases where a second layer existed, or a different medium was close to the illumination center, the reconstruction did not compare well to the theoretical value. Because these are are the realistic illumination conditions, we suggested that a better approximation is needed in order to reconstruct the effective attenuation coefficient using optoacoustic imaging.

References

[1] E.Salomatina B.Jiang J.Novak A.N.Yaroslavsky. "Optical properties of normal and cancerous human skin in the visible and near-infrared spectral range". In: *Biomed Opt* 11.6 (2006).

[2] B.E. Treeby B.T. Cox. "k-Wave: MATLAB toolbox for the simulation and reconstruction of photoacoustic wave fields". In: *Journal of Biomedical Optics* 15.2 (2010), p. 021314. DOI: 10.1117/1.3360308.

[3] A.Rosenthal V.Ntziachristos D.Razansky. "Acoustic Inversion in Optoacoustic Tomography: A Review". In: *Current Medical Imaging Reviews* 9 (2013), pp. 318–336.

[4] Grzegorz Domański et al. "A Simple Method of Determining the Effective Attenuation Coefficient". In: *Polish Journal of Medical Physics and Engineering* 13.1 (2007), pp. 1–12. ISSN: 1425-4689. DOI: 10.2478/v10013-007-0001-x. URL: http://www.pjmpe.waw.pl.

[5] P.Oltulu B.Ince N.Kokbudak S.Findik F.Kilinc. "Measurement of Epidermis, Dermis, and Total Skin Thicknesses from Six Different Body Regions with a New Ethical Histometric Technique". In: *Turkish Journal of Plastic Surgery* 26.2 (2018), pp. 56–61.

[6] T.Schröter R.Falz M.Busse J.Hoffman J.Thiele S.Kwast M.A.Borger. "Measurement of subcutaneous fat tissue: reliability and comparison of caliper and ultrasound via systematic body mapping". In: *Sci Rep* 12 (Sept. 2022).

[7] S.A. Prahl et al. "A Monte-Carlo Model of Light Propagation in Tissue". In: *Dosimetry of Laser Radiation in Medicine and Biology*. Vol. IS 5. SPIE Institute Series. SPIE, 1989, pp. 102–111.

[8] S.R.Arridge. "Optical tomography in medical imaging". In: *Inverse Problems* 15.2 (Apr. 1999), pp. 41–93.

8 Appendix

.1 Finite illumination

For a finite illumination, with radius R, the solution for the diffusion approximation will be:

$$U(r) = -\frac{1}{2D\mu_{eff}} \left(e^{-\mu_{eff}\sqrt{(x-l)^2+\rho^2}} - e^{-\mu_{eff}\sqrt{(x+l+2D)^2+\rho^2}} \right) \Bigg|_0^\infty \tag{6}$$

$$U(r) = \frac{1}{2D\mu_{eff}} \left(e^{-\mu_{eff}|x-l|} - e^{-\mu_{eff}\sqrt{(x-l)^2+R^2}} - e^{-\mu_{eff}|x+l+2D|} + e^{-\mu_{eff}\sqrt{(x+l+2D)^2+R^2}} \right) \tag{7}$$

$$U(r) = \frac{1}{2D\mu_{eff}} \left(e^{-\mu_{eff}|x-l|} - e^{-\mu_{eff}|x-l|\sqrt{1+\left(\frac{R}{x-l}\right)^2}} - e^{-\mu_{eff}|x+l+2D|} + e^{-\mu_{eff}|x+l+2D|\sqrt{1+\left(\frac{R}{x+l+2D}\right)^2}} \right) \tag{8}$$

We will assume that we mainly observe the first exponent. This is true, as for $x > l$ we get that $x - l < x + l + 2D$. If we didn't do this approximation, we couldn't find a lower bound for R.

$$U(r) = \frac{1}{2D\mu_{eff}} \left(e^{-\mu_{eff}|x-l|} - e^{-\mu_{eff}|x-l|\sqrt{1+\left(\frac{R}{x-l}\right)^2}} \right) \tag{9}$$

$$U(r) = \frac{1}{2D\mu_{eff}} e^{-\mu_{eff}|x-l|} \left(1 - e^{-\mu_{eff}|x-l|\left(\sqrt{1+\left(\frac{R}{x-l}\right)^2}-1\right)} \right) \tag{10}$$

.1.1 Normalized Fluence Error

The difference from the solution with an infinite illumination radius:

$$\Delta U = |U_\infty(r) - U_R(r)| = \frac{1}{2D\mu_{eff}} e^{-\mu_{eff}|x-l|\left(\sqrt{1+\left(\frac{R}{x-l}\right)^2}-1\right)} \tag{11}$$

After normalization:

$$\Delta U = e^{-\mu_{eff}|x-l|\left(\sqrt{1+\left(\frac{R}{x-l}\right)^2}-1\right)} \tag{12}$$

Now, we can force a maximal error, meaning $\Delta U < \epsilon$

$$e^{-\mu_{eff}|x-l|\left(\sqrt{1+\left(\frac{R}{x-l}\right)^2}-1\right)} < \epsilon \tag{13}$$

$$\sqrt{1+\left(\frac{R}{x-l}\right)^2} > 1 - \frac{\ln\epsilon}{\mu_{eff}|x-l|} \tag{14}$$

Of course $e < 1$.

$$\left(\frac{R}{x-l}\right)^2 > \left(1 - \frac{\ln\epsilon}{\mu_{eff}|x-l|}\right)^2 - 1 \tag{15}$$

$$\left(\frac{R}{x-l}\right)^2 > \left(\frac{\ln\epsilon}{\mu_{eff}|x-l|}\right)^2 - 2\frac{\ln\epsilon}{\mu_{eff}|x-l|} \tag{16}$$

$$R^2 > \left(\frac{\ln\epsilon}{\mu_{eff}}\right)^2 - 2\frac{\ln\epsilon}{\mu_{eff}}|x-l| \tag{17}$$

We are interested in areas where $x > l$:

$$R^2 > \left(\frac{\ln\epsilon}{\mu_{eff}}\right)^2 - 2\frac{\ln\epsilon}{\mu_{eff}}(x-l) \tag{18}$$

We recall that $\ln \epsilon$ is negative, therefore, the larger the x the larger we would need R. This makes sense, as the farther we are from the illumination, the smaller it is in the field of view, and the worse the infinite assumption is. Also, the smaller the the attenuation coefficient, the larger we would need R to be.

For the values in our simulations, Figure 14 describes the error as a function of the light source radius for different locations x.

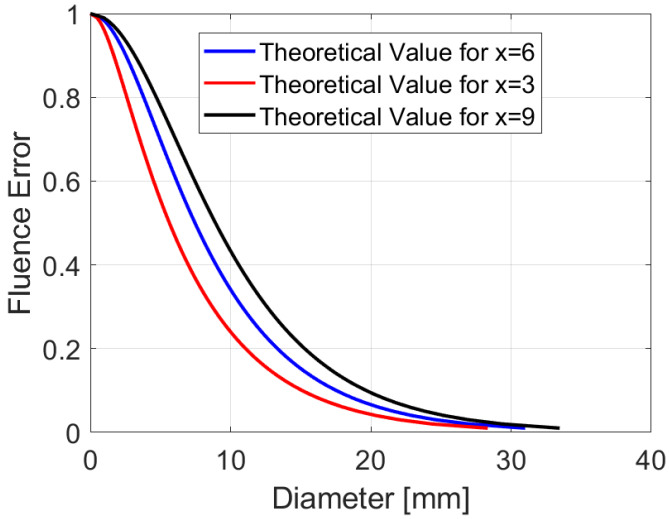

Figure 14: The normalized fluence error as a function of the light source diameter, for different depths x.

.1.2 Regression Error

More interesting to us than the fluence error, would be the error in our regression. Practically, the regression performs:

$$\mu_{eff} = -\frac{d}{dx}U$$

Therefore, we will perform this on our found finite illumination fluence, to find the expected slope. This will only be an approximation, as the slope changes in the regression area.

$$-\frac{d}{dx}U = \mu_{eff} - \frac{d}{dx}\log\left(1 - e^{-\mu_{eff}|x-l|\left(\sqrt{1+(\frac{R}{x-l})^2}-1\right)}\right)$$

$$-\frac{d}{dx}U = \mu_{eff} - \mu_{eff}\frac{\left(e^{-\mu_{eff}|x-l|\left(\sqrt{1+(\frac{R}{x-l})^2}-1\right)}\right)}{1 - e^{-\mu_{eff}|x-l|\left(\sqrt{1+(\frac{R}{x-l})^2}-1\right)}}\frac{d}{dx}\left(\sqrt{(x-l)^2+R^2} - (x-l)\right)$$

$$-\frac{d}{dx}U = \mu_{eff}\left[1 - \frac{\left(e^{-\mu_{eff}\sqrt{(x-l)^2+R^2}}\right)}{1 - e^{-\mu_{eff}\sqrt{(x-l)^2+R^2}}}\left(\frac{x-l}{\sqrt{(x-l)^2+R^2}} - 1\right)\right]$$

Therefore, the relative error would be:

$$\delta\mu_{eff} = \frac{\left(e^{-\mu_{eff}\sqrt{(x-l)^2+R^2}}\right)}{1 - e^{-\mu_{eff}\sqrt{(x-l)^2+R^2}}}\left(\frac{x-l}{\sqrt{(x-l)^2+R^2}} - 1\right)$$

Several plots of this can be seen in Figure 15. We can notice that for a large diameter, the variance in x is not high, and thus the slope is quite constant. Therefore, we expect this to be the actual error. For small diameter the variance is high, and this approximation does not hold. This fits the results in Figure 1.

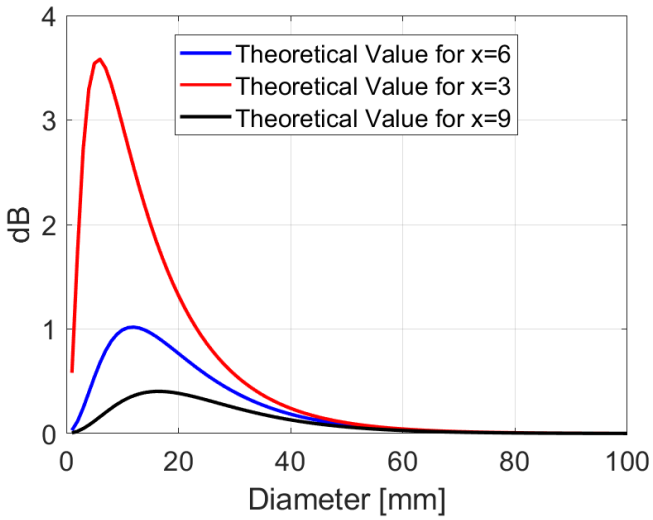

Figure 15: The regression error as a function of the light source diameter, for different depths x.